

# Integrating State of the Art Compute, Communication, and Autotuning Strategies to Multiply the Performance of the Application Program CPMD for *Ab Initio* Molecular Dynamics Simulations

Tobias Klöffel<sup>a,b</sup>, Gerald Mathias<sup>c</sup>, Bernd Meyer<sup>a,\*</sup>

<sup>a</sup>Interdisciplinary Center for Molecular Materials (ICMM) and Computer-Chemistry-Center (CCC), Friedrich-Alexander-Universität Erlangen-Nürnberg (FAU), Nägelsbachstraße 25, 91052 Erlangen, Germany

<sup>b</sup>High Performance Computing Group, Regional Computing Center Erlangen (RRZE),

Friedrich-Alexander-Universität Erlangen-Nürnberg (FAU), Martensstraße 1, 90158 Erlangen, Germany

<sup>c</sup>Leibniz Supercomputing Centre of the Bavarian Academy of Sciences and Humanities, Boltzmannstr. 1, 85748 Garching, Germany

## Abstract

We present our recent code modernizations of the of the *ab initio* molecular dynamics program CPMD ([www.cpmc.org](http://www.cpmc.org)) with a special focus on the ultra-soft pseudopotential (USPP) code path. Following the internal instrumentation of CPMD, all time critical routines have been revised to maximize the computational throughput and to minimize the communication overhead for optimal performance. Throughout the program missing hybrid MPI+OpenMP parallelization has been added to optimize scaling. For communication intensive routines, as the multiple distributed 3-*d* FFTs of the electronic states and distributed matrix-matrix multiplications related to the  $\beta$ -projectors of the pseudopotentials, this MPI+OpenMP parallelization now overlaps computation and communication. The necessary partitioning of the workload is optimized by an auto-tuning algorithm. In addition, the largest global MPI.Allreduce operation has been replaced by highly tuned node-local parallelized operations using MPI shared-memory windows to avoid inter-node communication. A batched algorithm for the multiple 3-*d* FFTs improves the throughput of the MPI.Alltoall communication and, thus, the scalability of the implementation, both for USPP and for the frequently used norm-conserving pseudopotential code path. The enhanced performance and scalability is demonstrated on a mid-sized benchmark system of 256 water molecules and further water systems of from 32 up to 2048 molecules.

**Keywords:** CPMD, *ab initio* molecular dynamics, hybrid parallelization, overlapping computation and communication, batched 3-*d* FFT

## 1. Introduction

The field of *ab initio* molecular dynamics (AIMD) has been enormously growing over more than two decades providing exciting new insights to chemistry and materials science at atomic resolution. In AIMD atoms are propagated in time according to Newton's equations of motion to study physical properties and chemical reactions of molecules and condensed phase systems at finite temperature.[1, 2] The necessary energies and forces are derived from first principles quantum chemistry, whose enormous computational effort has made it a key application in high-performance computing (HPC).

One of the most successful implementations of AIMD is the CPMD[3] code, which has been available on almost all major HPC platforms since the late 1990'. The code is MPI[4] parallel and offers a OpenMP[5] parallelization on top for many time critical routines.

A key factor to its success always was the porting and optimization for new compute architectures, like vector machines

or the multi-core architecture of the IBM Blue Gene series. More recent porting efforts focus on the support of accelerators, namely GPUs [6], which are one aspect of a general trend in high performance computing. In the last decade, the compute power but also the complexity of the nodes has grown much stronger than the speed of the interconnects. On current supercomputers each node typically hosts dozens of of cores with strong vector units, and the cores may be complemented by GPU accelerators. The intra-node communication between these units is by an order of magnitude faster than the inter-node network.

The underlying method of CPMD is Kohn-Sham density functional theory (DFT), which describes the electrons through singly or doubly occupied electronic states. In CPMD these states are expanded in a plane-wave (PW) basis and propagated via the Car-Parrinello extended Lagrangean technique. For details of the method and the implementations see [1, 2].

Some properties of the electrons are calculated efficiently in momentum space, other operators are diagonal in real space. CPMD uses 3-*d* fast Fourier transforms (FFT) to switch back and forth between these two representations for a most efficient computation [1, 7, 8]. Thus, the key objects of the method are the grids in real and momentum space that are used to represent

\*Corresponding author.

Email addresses: [tobias.kloeffel@fau.de](mailto:tobias.kloeffel@fau.de) (Tobias Klöffel), [gerald.mathias@lrz.de](mailto:gerald.mathias@lrz.de) (Gerald Mathias), [bernd.meyer@fau.de](mailto:bernd.meyer@fau.de) (Bernd Meyer)

the electron density in the simulation cell, the core potentials and the electronic states.

CPMD uses so-call pseudopotentials (PP) to describe the chemically inert core electrons and to limit the calculation to the valence electrons [9]. This restriction requires a much smaller plane-wave basis than one would need for an all-electron calculation. For the frequently used norm-conserving PP (NCPP) this results in real space grids of a few hundred points per dimension for the FFT. The resolution of the grid can be further reduced by at least 40 % by using Vanderbilt ultra-soft PP (USPP) [10].

The USPP method is formulated in  $N$  electronic states  $\{|\phi_i\rangle\}$ , which fulfill the constraint

$$\langle \phi_i | S | \phi_j \rangle = \delta_{ij} \quad (1)$$

by means of the non-local overlap operator

$$S = 1 + \sum_{l,mn} q_{mn}^l |\beta_m^l\rangle \langle \beta_n^l|, \quad (2)$$

which depends on the  $\beta$ -projectors  $\{|\beta_m^l\rangle\}$  of the atoms  $\{I\}$  and the integrals

$$q_{mn}^l = \int d\mathbf{r} Q_{mn}^l(\mathbf{r}) \quad (3)$$

of the augmentation functions  $Q_{mn}^l(\mathbf{r})$  provided with the USPPs.[10, 11]. These augmentation functions are also required to compute the total electron density

$$n(\mathbf{r}) = \sum_i \left[ |\phi_i(\mathbf{r})|^2 + \sum_{mn,l} Q_{mn}^l(\mathbf{r}) \langle \phi_i | \beta_n^l \rangle \langle \beta_m^l | \phi_i \rangle \right], \quad (4)$$

which contains contribution from the projections of the  $|\phi_i\rangle$  onto the USPP.

The non-local overlap operator (2) leads to the generalized eigenvalue problem

$$H|\phi_i\rangle = \epsilon_i S|\phi_i\rangle \quad (5)$$

for the time independent Schrödinger equation with the Hamiltonian

$$H = -\nabla^2 + V^{\text{eff}} + \sum_{mn,l} D_{mn}^l |\beta_m^l\rangle \langle \beta_n^l|, \quad (6)$$

where the last term containing

$$D_{mn}^l = D_{mn}^{(0)} + \int d\mathbf{r} V^{\text{eff}}(\mathbf{r}) Q_{mn}^l(\mathbf{r}) \quad (7)$$

describes the non-local part of the potential with given parameters  $D_{mn}^{(0)}$ .

Because the generalized constraint (1) is difficult to handle in the extended Lagrangean dynamics of CPMD [11] a set of orthogonal orbitals  $\{|\psi_i\rangle\}$  is used,[12] which yield the original

$$|\phi_i\rangle = \sum_j |\psi_j\rangle T_{ij}, \quad (8)$$

by the inverse root  $T = O^{-1/2}$  of the overlap

$$O_{ij} = \langle \psi_i | S(\{\mathbf{R}_I\}) | \psi_j \rangle. \quad (9)$$

Potential energies and forces are still calculated with respect to the  $\{|\phi_i\rangle\}$ , which requires frequent transformations between these two representations.

In CPMD the orthonormality of the  $\{|\psi_i\rangle\}$  is not enforced by the full set of  $N^2$  coupled constraints  $\langle \psi_i | \psi_j \rangle - \delta_{ij} = 0$ , but just by the  $N$  diagonal constraints  $\langle \psi_i | \psi_i \rangle - 1 = 0$ , which are decoupled and, thus, their Lagrangean multipliers are easy to determine. On the downside orthogonality has to be enforced from time to time by solving an  $N^2$  eigenvalue problem.[12]

Using USPP, each atomic PP requires about twice as many  $\beta$ -projectors as NCPP to map the interaction of the atomic core with the electronic states [11]. The larger number of  $\beta$ -projectors together with the additional terms appearing in the equations above, the USPP scheme requires some extra computation. Ideally, this should be more than compensated by the lower grid resolution and much smaller plane wave basis set (roughly a factor of eight). Also from a parallelization standpoint, bearing in mind the above discussion on the fast growth of the nodes computational power, the USPP approach seems favorable compared to NCPP, since it reduces the amount of communication at the expense of some extra computation. However, in the current implementation of CPMD the USPP code branch is only slightly faster than NCPP and displays rather poor scaling. Nevertheless, USPP calculations in CPMD have been indispensable for systems with a large number of electrons because the much smaller basis set largely reduces memory requirements [11].

The heart of data parallelization in CPMD is a 1- $d$  domain decomposition of the FFT grid, i.e. the  $yz$ -planes of the electron density are distributed to the MPI tasks (see [1, 2] for details). Thus, the few hundred grid points per dimension is an effective limit for the number of MPI tasks that can be efficiently used in a calculation. A decade ago, this was not critical on most HPC platforms, but with the emergence of powerful multi- and many-core compute nodes pure MPI parallelization limits the achievable performance of the code. CPMD already can be operated in a hybrid MPI+X mode, where additional thread parallelization is introduced via performance libraries (BLAS, LAPACK, FFT)[13, 14, 15] and explicit OpenMP[16] directives. However, not all code paths are equally well thread parallelized and the efficiency of CPMD in hybrid mode often falls behind that of pure MPI. This problem is particularly pressing for simulations that use USPP due to the much smaller FFT grid. Concomitantly, USPP use a much smaller spacial grid and reach the scaling limit in a pure MPI mode earlier. On top, the hybrid parallelization scheme is not as well maintained for the USPP code path as for norm-conserving PPs.

Recently, a second level of MPI parallelization was introduced in CPMD to enhance the scalability [17]. In the so-called `cp_groups` parallelization, the MPI tasks with their associated memory shares are replicated  $g$  times. Each of these  $g$  `cp_groups` computes the same workload per default. For speed-up, the members with the same index in different `cp_groups` do work-sharing and data synchronization among each other. Originally, this was implemented to distribute state pairs for exact exchange and to parallelize the FFT routines over the electronic states. For all USPP specific routines these

`cp_groups` parallelization has been missing completely.

In this paper we discuss our latest revision of the CPMD code to alleviate the parallelization and performance bottlenecks of the USPP code path. It builds upon our intermediate results presented at the Supercomputing Conference 2018.[18] On node level our effort aims to fully exploit the powerful compute units of current machines and make use of the fast intra-node communication with hybrid MPI+OpenMP parallelization strategies. Furthermore, we address the time critical parallel tasks, namely the distributed matrix-matrix multiplication to calculate the overlap of the electronic states with the  $\beta$ -projectors and the 3-*d* FFT of the electronic states. For both routines, respectively, we introduce overlapping computation and communication to reduce the communication overhead. The required data partitioning strategy is determined by an auto-tuning algorithm. Where possible, inter-node communication is avoided by node local parallelization, using e.g. MPI shared-memory windows. To achieve maximum scaling we complemented compute routines by a `cp_groups` parallelization scheme where applicable.

The following Methods section gives an overview of the systems used for benchmarking before we describe details of the code changes in the section Optimization. The benefits of our efforts are discussed in the section Results and a short Summary and Outlook concludes the paper.

## 2. Methods

Starting point for our optimization was the development version of CPMD (current release version is 4.3). CPMD brings its own instrumentation to measure routine timings inclusive and exclusive the timing of subroutines. For the optimization of selected routines we have used this instrumentation to measure the timing of individual code blocks, as well. Furthermore, CPMD measures the amount of data and the bandwidth in MPI communications, which supported the optimization of communication. The external tools used for performance measurements and optimization were `likwid`[19], `PerSyst`[20] and the `optreport` option of the Intel FORTRAN compiler,[21] which helped us to check if certain loops have been SIMD vectorized.

We will exemplify our optimization progress on a benchmark system of 256 water molecules, which lies in a medium system size range between 500 and 2000 electronic states used in many state of the art AIMD publications [22, 23, 24, 25, 26].

Molecules were simulated enclosed in a  $19.734^3 \text{ \AA}^3$  periodic box with a PW cut off of 25 Ry and a time step of 6 a.u., employing the PBXE functional[27] including Grimme's D3 correction[28] for long range dispersion interactions. This system comprises 1024 electronic states, which are expanded in 54564 PW basis functions. The USPP of the Oxygen atoms contain eight projectors each; Hydrogen atoms covers one  $\beta$ -projector, which leads to a total of 2560  $\beta$ -projectors. Hydrogen masses were set to 2 a.m.u. and the fictitious electron mass was 700 a.u. The CPMD code was compiled with the Intel compiler suite 2019, including Intel MPI and Intel MKL [21, 29, 30]. The latter was used both for BLAS/LAPACK calls and for FFT. ELPA 2019.05 was compiled with the same Intel compilers[31].

For comparison with the NCPP code path, we also benchmarked the same 256 water molecule system with the NCPP implementation of CPMD. Here we used Trouiller-Martins norm-conserving PPs [32] with a PW cutoff of 80 Ry, which results in 313126 PW basis functions. Since only the 2S-spin channel of Oxygen needs a  $\beta$ -projector, 256  $\beta$ -projectors are included in the NCPP calculation.

We also conducted scaling tests with system sizes 32, 64, 128, 256, 512, 1024 and 2048 water molecules, respectively. The initial simulation cells are taken from CP2K.org [33].

For the performance measurements we have run 1000 steps of Car-Parrinello MD and evaluated the average time per step. IO was excluded because it is typically not a bottleneck for production runs but reading/writing the restart (checkpoint) files can significantly add to the timings of the benchmark runs. We checked the reproducibility of measured timings by repeating the benchmark runs and found standard deviations of less than 0.5%, which was sufficient for our purposes. Newly implemented auto-tuning algorithms were performed during the initialization phase and do not contribute to the overall timing.

The benchmarks simulations were run on SuperMUC-NG, whose nodes feature  $2 \times 24$  cores Intel® Skylake Xeon Platinum 8174 processors running at 2.3 GHz and 96 GB of memory (80 GB usable). The nodes of an island are interconnected by a fully non-blocking fat tree 100 Gbit/s Intel® OmniPath network. For our benchmarks we always constrained the nodes to be on the same island. Up to 384 nodes were used for a single simulation. For hybrid MPI/OpenMP runs we benchmarked 1, 2, 3, 4, 6, 8, 12, or 24 OpenMP tasks per MPI thread to evenly fill each node. `cp_groups` parallelization was benchmarked with up to eight `cp_groups`.

For comparison, we benchmarked both the original CPMD 4.3 code and our revised code. For the former, however, we omitted the `cp_groups` parallelization in the USPP benchmarks, since it was only implemented for the FFT.

## 3. Optimization

Working through the list of the most time-consuming routines in CPMD we managed to eliminate many bottlenecks. A first focus lay on the node-level optimization for enhanced performance. As we show below, some routines were speed up by one or two orders of magnitude through performance libraries, OpenMP parallelization and optimization of memory access patterns, such that these routines became less important or even negligible in the overall timing.

The second focus was to improve the scalability within the target hybrid MPI+OpenMP parallelization. Here, for the two most time-critical routines we have revised the respective parallel communication pattern.

### 3.1. Overlap of $\beta$ -projectors

The largest computational effort with respect to matrix-matrix multiplication and a major computational bottleneck in the USPP code path of CPMD is the computation of the overlaps

$$F_{l,m,i}^{\text{NL}} = \langle \beta_m^l | \phi_i \rangle \quad \text{and} \quad \tilde{F}_{l,m,i}^{\text{NL}} = \langle \beta_m^l | \psi_i \rangle \quad (10)$$

of the  $\beta$ -projectors and the two sets of electronic states, which are core quantities for the USPP code path due to their size. It requires a summation over the PW coefficients, who, for the electronic states, are distributed among the MPI tasks. Thus, the partial sums to  $F^{\text{NL}}$  from each task are combined by an MPI `Allreduce` operation.

The computation of these overlaps is implemented in the routine `rn1sm1`, which calls `DGEMM` for each  $\beta$ -projector of each atomic species. `rn1sm1` is called twice in CPMD 4.3, once to calculate the projections on the orbitals  $\{|\psi_i\rangle\}$  used for the dynamics and a second time to calculate the projections on the orbitals  $\{|\phi_i\rangle\}$  used for evaluating ionic forces and electronic gradients. Since these two sets of orbitals are related by the transformation (8) we have eliminated the second call to `rn1sm1` and compute the second projection by the transform

$$F_{l,m,i}^{\text{NL}} = \sum_j \tilde{F}_{l,m,j}^{\text{NL}} T_{ij}. \quad (11)$$

For this new routine `rottr_fn1` we have chosen a node-local parallelization, where the work is distributed among the MPI tasks of each node, since the overall computational effort is small but not negligible. The node local tasks share data in a MPI shared-memory window, and, thus, avoid communication.

To optimize the remaining singular call to `rn1sm1`, we pack all  $\beta$ -projectors in a single matrix. A single call to `DGEMM` now is most efficient; in our benchmark system it has the large dimensions  $M = 2560$ ,  $N = 1024$ ,  $K = 54564$ , where the inner dimension  $K$  is the number of PW, which are distributed over the MPI tasks. The partial contributions are summed over the tasks by MPI `Allreduce` after the computation, which amounts to 20 MB in our benchmark and hampers scaling. To improve the scaling and the overall timing the new implementation subdivides the  $\beta$ -projector matrix into  $n$  buffers, which serve to overlap computation and communication.

Figure 1 sketches the resulting algorithm for the choice  $n = 3$ . First, all threads compute the local contribution of buffer 1 to  $F^{\text{NL}}$ . This is done to reduce the impact of splitting off a complete thread and dedicate this thread to the MPI communication, which is done after performing the first `DGEMM`. The master thread then conducts the MPI `Allreduce` operation, while the remaining worker threads continue evaluating buffers 2 to  $n$ . When the communication is finished, the buffer content is copied to the internal data structure in CPMD. To enable further scaling, we adopted the `cp_groups` parallelism to distribute the  $\beta$ -projectors between the groups.

Choosing an optimal  $n$  and the relative buffer sizes of buffer 1 and buffers 2 to buffer  $n$  strongly depends on the number of threads, the performance of the processor and network architecture. Therefore, we implemented an auto-tuning algorithm, which measures the relative timing of computation and communication during the first few MD steps and chooses an optimal set-up.

Performance and scalability improvements of the revised algorithm are presented in Figure 2. Here, the node level opti-

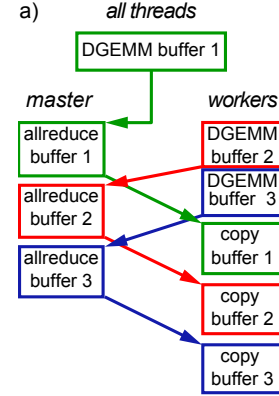


Figure 1: Revised algorithm for `rn1sm1` for  $n = 3$  implementing overlapping computation and communication.

mization of the `rn1sm1` routine yields a speedup of about 1.7 on a single node (48 cores). Up to 8 nodes (384 cores) the new algorithm displays excellent scaling and is more than 3.0 times faster than the original implementation. Since the node-local rotation is almost negligible the overall performance improvement is about a factor of 5.3. Beyond 8 nodes the overall timing reaches a plateau until at 32 nodes the first data point with `cp_groups` parallelism is presented, leading to a sizable improvement. From Fig. 2 it may look appealing to use `cp_groups` parallelization already for fewer nodes, but it requires additional synchronizations events throughout the code. Even though we have minimized this synchronization of the `cp_groups`, the overall performance of the code benefits from this additional parallelization level only at 1536 cores and beyond for our test system, where it enables further scaling of the algorithm.

The choice of replacing the second call to `rn1sm1` with the node local `rottr_fn1` is clearly beneficial as the total time is now dominated by the single `rn1sm1` call. Also the parallelization of `rottr_fn1` with an MPI shared memory window is working exceptionally well. Despite of different numbers of OpenMP threads at the various node counts, the routine shows an almost constant timing. Due to `cp_groups` parallelism the node local workload is reduced at core counts beyond 3072 cores and the timing is sped up. For a detailed comparison of number of cores and OpenMP threads per MPI task see Tab. 4.1 below. For larger systems, however, this scaling limit will manifest much later because the computational effort grows faster with the system size than the communication. The overlapping computation and communication is beneficial already upwards from two nodes and does not add any overhead for a single node.

### 3.2. Ionic Gradients of $\beta$ -Projectors

In contrast to Born-Oppenheimer MD, where ionic forces are evaluated once after an self-consistent field (SCF) cycle, Car-Parrinello MD requires ionic forces together with each update of the wave function. Therefore, force evaluation is a dominant part of the overall computational time. For the forces due to the  $\beta$ -projectors it requires the quantity

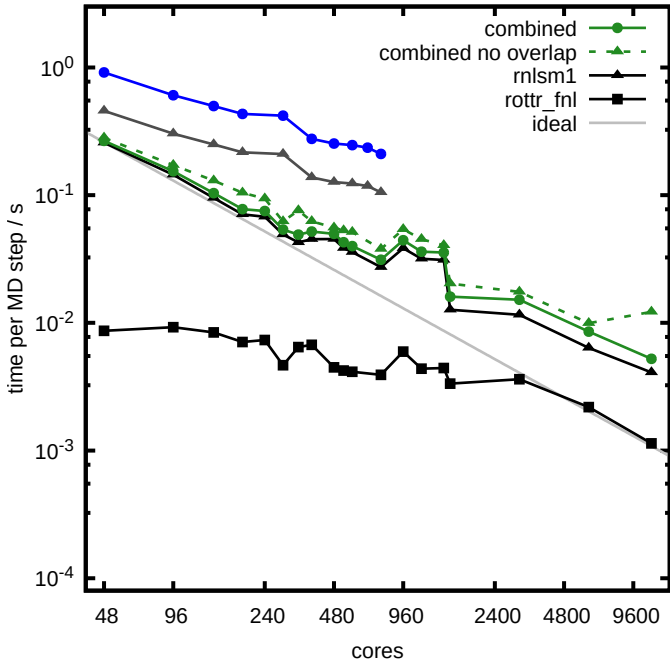


Figure 2: Routine specific and combined time spent to compute  $\tilde{F}^{\text{NL}}$  and  $F^{\text{NL}}$ . The grey line represents the routine `rn1sm1` of CPMD 4.3, which is called twice per time step; the combined time is shown in blue. The revised implementation calls `rn1sm1` once per MD step (black triangles) and substitutes the second call with `rottr_fn1` (black squares). Green shows the total time of the new implementation, green dashed shows the resulting timings if `rn1sm1` is used without overlapping communication and computation.

$$dF_{l,m,i}^{\text{NL}} = \langle \nabla_i \beta_m^l | \phi_i \rangle, \quad (12)$$

which is calculated in subroutine `rn1sm2`.

Finally, subroutine `rn1f1` calculates its contribution to the ionic forces. In the original implementation of `rn1sm2` each MPI task holds a slice of array  $dF_{l,m,i}^{\text{NL}}$  so that `rn1f1` evaluates forces due to these slices in parallel. Still, the effort is sizeable as `rn1f1` uses an eight-fold nested loop without any OpenMP parallelization. Thus, both `rn1sm2` and routines `rn1f1` are equally time consuming in CPMD 4.3, where the scaling of `rn1f1` was slightly better.

In a first step,[18] we have applied the same optimizations to `rn1sm2` as to `rn1sm1` described in Section 3.1. This led to a similar speed up and scaling, but still the cost for `rn1f1` was sizeable. Close inspection of `rn1f1` revealed that a large portion of the computational effort can be expressed by a matrix-matrix multiplication of  $F^{\text{NL}}$  to the Hamilton matrix

$$H_{i,j} = \langle \phi_i | H | \phi_j \rangle. \quad (13)$$

This product is not only required in `rn1f1` but also in the routine `nlforce`, which computes the gradients of the electronic states and will be discussed in Section 3.3 below. We have implemented this matrix-matrix multiplication in the new routine `rotate_fn1`, which uses the same parallelization strategy as in `rottr_fn1`. Using this intermediate quantity the revised `rn1f1` now is OpenMP parallel, uses SIMD vectorization, and is at node level about two orders of magnitude faster. Because

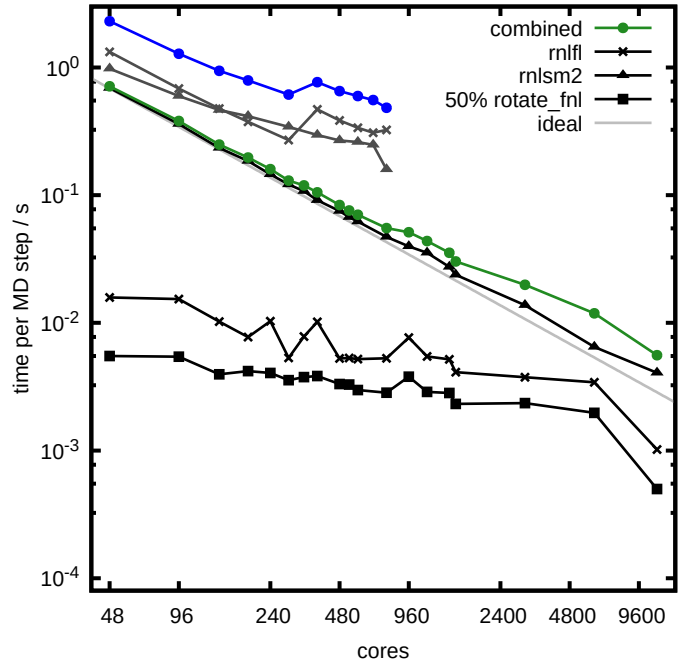


Figure 3: Time spent to compute the ionic gradients of the  $\beta$ -projectors. Grey and blue lines, respectively, represent the routines and combined timing of the old implementation in CPMD 4.3. Black and green lines, respectively, are the revised routines and combined timing of the new implementation. For `rotate_fn1` only half of the routine time is added to the combined time, the other half contributes to the gradients of the electronic states.

of this massive speed up of `rn1f1` its parallelization across MPI tasks is no longer necessary and we discard it. As a result, the reduction operation of  $dF^{\text{NL}}$  across the MPI tasks can be skipped, which makes `rn1sm2` communication free in the USPP code path. For our benchmark system this discards an `MPI_Allreduce` operation of  $3 \times 20$  MB in size.

The resulting timings for the ionic gradients due to the  $\beta$ -projectors are shown in Figure 3. As indicated above, the time spent in the new `rotate_fn1` and the revised `rn1f1` is almost negligible and both routines profit from `cp_groups` parallelization, which is active at large core counts. The overall time now is dominated by `rn1sm2`, which scales perfectly up to very large core counts, since no communication is involved. Similar to `rottr_fn1` in Fig. 2 the node local routines `rn1f1` and `rotate_fn1` contribute only very little to the overall timing. Only in the scaling limit of our benchmarks going beyond 3000 cores they have a noticeable impact on the combined timings.

### 3.3. Electronic Gradients of $\beta$ -Projectors

Electronic gradients are required for every wave-function update, either in a Car-Parrinello MD step or a Born-Oppenheimer MD SCF cycle. In CPMD the subroutine `nlforce` calculates the non-local contributions to the electronic gradient due to the  $\beta$ -projectors.

The implementation requires the same multiplication of  $H$  to  $F^{\text{NL}}$  as in the `rn1f1` routine. As indicated in Sec. 3.2, we use the result of this multiplication from the `rotate_fn1` routine and consider half its timing for the cost of the new implementation. The remaining computational effort in `nlforce` is

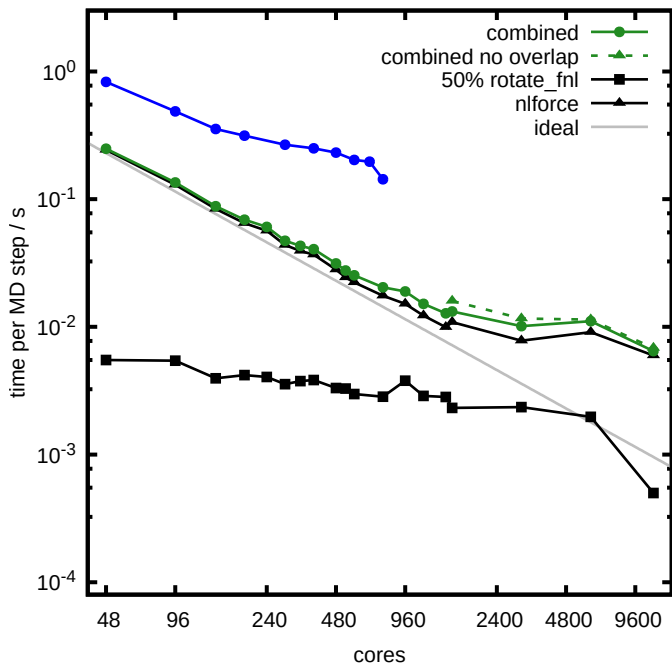


Figure 4: The blue curve shows the timing for `rn1f1` in the old implementation. In the new implementation reuses the quantity calculated in `rotate_fnl`. The combined time of the new algorithm is given by the green solid line. The green dashed line shows the combined time without overlapping communication and computation. The latter is only needed communication of the `cp_groups` parallelization.

a second matrix-matrix multiplication. In the old implementation, this multiplication was called for every  $\beta$ -projector of every atomic species, as in `rn1sm1` and `rn1sm2`. The new implementation uses a single compact matrix-matrix multiplication combining *all*  $\beta$ -projectors, and, thus, makes best use of thread and SIMD parallelization.

The matrix-matrix multiplication of the revised algorithm requires no communication, except when the newly added `cp_groups` parallelization is used. Here, the matrix-matrix multiplication is distributed among the `cp_groups` and data is synchronized by an `MPI_allgather`. The cost for the latter is reduced by an overlap of computation and communication, similar to the `rn1sm1` described in Figure 1.

The resulting speed up is demonstrated in Figure 4. For a single node the new implementation is almost three times faster. It scales perfectly up to 1536 cores. At this point `cp_groups` parallelization is activated and the effect of overlapping communication and computation to hide the synchronization between `cp_groups` is visible and keeps the algorithm scaling up to 2400 cores. At very high core counts the communication between `cp_groups` dominates and limits the scalability. Also the cost of `rotate_fnl` now contributes noticeable to the overall timings, similar as mentioned in Sec. 3.2.

### 3.4. Further USPP specific Optimizations

Working through the list of time consuming routines, we identified four additional routines of the USPP code path which consumed sizeable part of the total compute time in the original CPMD version. We have applied the same optimization

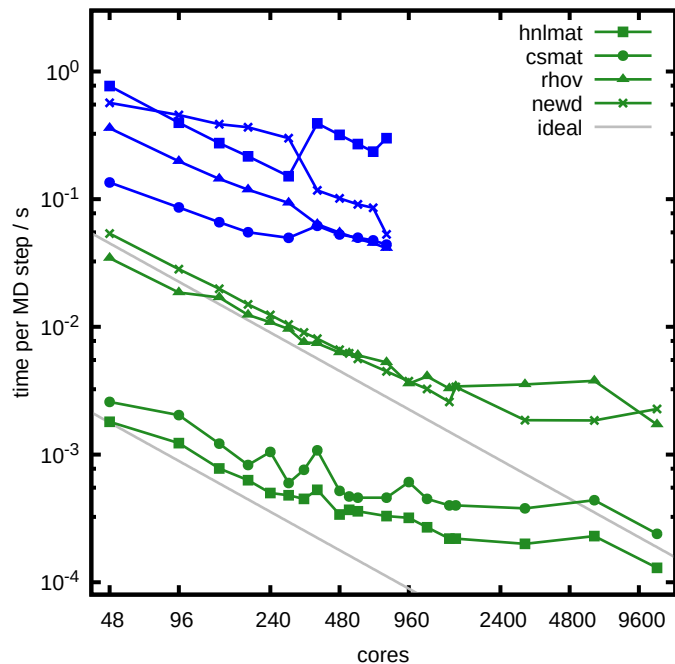


Figure 5: Reduction of the time per MD step for various routines (symbols) comparing CPMD 4.3 (blue lines) to the revised code version (green lines).

paradigms as for the routines above, namely targeting BLAS calls with large matrices, complementing missing OpenMP directives and adding additional `cp_groups` parallelization.

Figure 5 show the improvements of these four routines (green lines) with respect to CPMD 4.3 (blue lines). The routine `newd` (cross symbols) computes the integral part of (7) and its ionic gradients, if required. Here, we now store the components of  $Q^I$  instead of computing them on the fly in every time step. Together with improved matrix-matrix multiplications, this gives a speed up of about ten and the added `cp_groups` parallelization greatly improves the scalability. Saving the  $Q^I$  additionally speeds up the computation of the augmentation-charge density, which adds to the square of the wave function in the computation of the total charge density in (4). The corresponding routine `rhov` also becomes significantly faster and scales similar as `newd`.

The largest speed-up of almost three orders of magnitude was achieved for the routine `hn1mat` (square symbols), which computes the nonlocal part of the Hamiltonian matrix  $H$  (13) stemming from the sum expression in (6). In the original algorithm the respective matrix elements have been updated in the innermost part of a nested loop construct. Originally, the routine was MPI parallelized by distributing the matrix elements of state pairs  $i \leq j$  across the MPI tasks. In the revised implementation, we now distribute contributions of the different atoms to the MPI tasks and compute the partial contributions of an atom to all state pairs within an MPI tasks. Thereby, we could replace a complicated nested loop construct by a single and compute efficient DGEMM call. Now this routine is essentially negligible with respect to the total timing ( $< 0.1\%$ ). Similarly, we have rewritten the `csmat` routine (dot symbols), which computes the overlap matrix  $O$  (9). The resulting timings are now compar-

ble to the `hn1mat` and equally do not play a role in the overall timing any more.

### 3.5. Batched Multi 3-d FFT

One of the main computational bottlenecks in CPMD are the 3-d FFTs needed to transform the electronic states (1024 for our 256 water benchmark) from momentum space to real space. The states in real space are needed twice per MD step, once for the calculation of the electronic density (4) and once for the interaction with the effective potential  $V^{\text{eff}}$  (6). Subsequently, the product of the wave function with  $V^{\text{eff}}$  is transformed from real to momentum space to calculate the gradients on the electronic states. Since the coefficients of each state are distributed over the MPI tasks, an *all-to-all* communication is required for every single transform.

In the continuous development of CPMD (and many other PW AIMD codes) huge effort has been spent on the improvement of the 3-d FFT algorithm. In CPMD the current implementation of 3-d FFT treats only non-zero values explicitly in the FFT.[34] As back ends for the actual 1-d FFT performance libraries such as FFTW or MKL can be used.[35, 29]

For the backward FFT of each of the  $N$  electronic states to real space, one needs first a FFT in  $z$  direction, an `MPI_Alltoall` communication step, and then the FFTs in  $y$  and  $x$  direction. The execution of the FFT for the three stencil directions is the computationally demanding part, whereas the *all-to-all* communication is the major bottleneck for scalability. Here, large MPI task counts lead to small message sizes which largely reduce the effective bandwidth of the communication.

A straight forward strategy for optimization is to have fewer communication steps with larger message sizes. For the multiple 3-d FFTs we achieve this by packing the communication from multiple electronic states, thus, implementing a batched multi 3-d FFT algorithm. Accordingly, we have rewritten all 3-d FFT routines such that each of the individual steps is executed for  $b$  states and uses a buffer of  $b$  times the size of the original one, where  $b$  is the batch size. Thereby, the message size of the *all-to-all* communication is  $b$ -fold increased and the number of communication calls is  $b$ -fold reduced. Furthermore, also  $b$ -times as many stencils are transformed in a single call to the FFT library. This is particularly beneficial in a hybrid MPI/OpenMP parallelization scheme, where a threaded FFT is used and the individual FFTs are distributed among many cores.

Similar to the matrix-matrix multiplications in Sec. 3.1 we have, furthermore, extended the batched 3-d FFT algorithm to overlap computation and communication, see Figure 6. Here, we use two buffers  $A$  and  $B$  that are alternated for and even indexed batches.

After finishing the  $z$  FFT of the first batch in buffer  $A$  by the worker threads, the local master thread starts its *all-to-all* communication of buffer  $A$ .

Concurrent to this communication, the workers compute the  $z$  FFT of batch 2 in buffer  $B$ . After the master finishes the *all-to-all* communication of buffer  $A$  control is handed over to the worker threads, which compute the  $y$  and  $x$  FFTs of batch 1. Then the result is stored and buffer  $A$  is refilled by the  $z$  FFT of

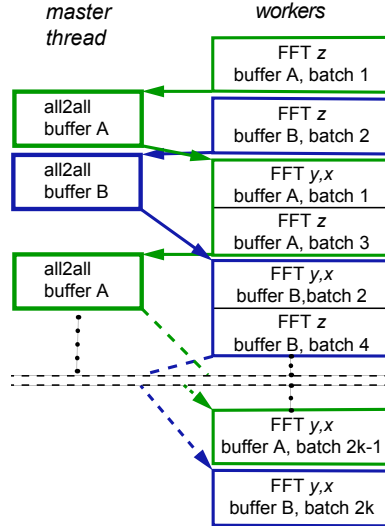


Figure 6: Program flow of the batched 3-d FFT with overlapping computation and communication applied to the electronic states from momentum space to real space. Batches with odd index use buffer  $A$ , buffers with even index use buffer  $B$ .

batch 3. Both master and worker threads alternate working on buffers  $A$  and  $B$ . As long as communication of a batch is shorter than the computation of its three fold FFT, the worker threads are constantly busy.

Choosing a sufficiently large batch size  $b$  to saturate the bandwidth depends on the simulation system and the machine it runs on. Here, we have implemented an auto-tuning algorithm that scans through the possible values of  $b$  and determines the fastest setting. For our benchmark system we observe batch sizes from  $b = 1$  to  $b = 43$  with the expected general trend that for more MPI tasks in each of the `cp_groups` larger  $b$  are preferred.

Finally, we omit the second call of the FFT to real space by storing the transformed wave functions after the first call. This functionality has already been implemented in CPMD but was inactive in the USPP code branch. For our benchmark system, the total memory required to store the wave functions in real space is 13.5 GB. Storing and retrieving this data will be generally faster than the FFT it replaces but still is not negligible in the overall timing due to its size.

Since the original USPP implementation was not OpenMP parallel, we decided to demonstrate the capabilities of the original FFT implementation using our new implementation together with the old FFT implementation and compare it to our new batched FFT routines in Fig. 7.

The old implementation shows a good scalability up to 384 cores, where the performance reaches a plateau. At 1536 cores the effect of `cp_groups` parallelism is clearly visible, and enables further scaling of the algorithm. Again we have to note that the synchronization triggered by `cp_groups` parallelization is non-negligible as already mentioned in Section 3.1.

Compared to the original implementation our batched FFT routines show better scalability, if overlapping communication

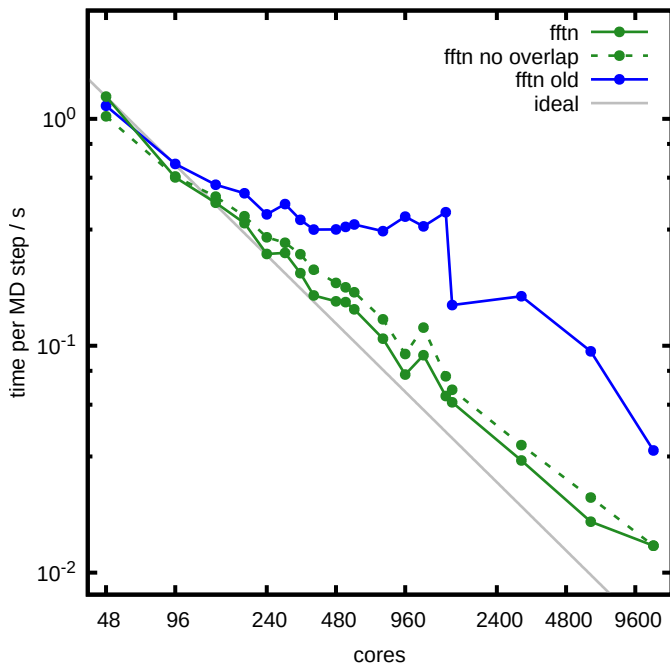


Figure 7: Total time spent in FFT with increasing core counts. Blue shows the old implementation, green the new batched algorithm and green dashed the new algorithm without overlapping communication and computation.

and computation is enabled, the routine scales well up to 960 cores. At this point the batched 3- $d$  FFT is roughly a factor of 5 faster than the old implementation. At 1536 cores we can also observe a speedup due to the `cp_groups`, however, the impact is much less than in the original implementation. This excellent scaling without `cp_groups` parallelization is needed up to 1536 cores avoids additional MPI communication due to data synchronization and has a large impact on the overall scalability of the code. For larger node counts the new algorithm continues to scale up to 9600 cores and retains a sizable speedup compared to the old code.

The effect of overlapping communication and computation is visible comparing the solid and dashed green lines. It is in the expected range, since one thread exclusively handles the communication. Thus the performance of the computational part is reduced by a factor of  $1/n$ , where  $n$  is the number of OpenMP threads. Since in our benchmark system we found 12 OpenMP threads to be most efficient for almost all core counts, the unavoidable performance loss is 8.3%. Yet we see a overall performance improvement in the range of 20 - 30% indicating the effectiveness of our implementation.

### 3.6. USPP Eigenvalue Problem

Going to large node counts, one major scaling problem turned out to be solving of the symmetric  $N \times N$  eigenvalue problem in each MD step to restore the orthogonality of the  $\{|\psi_i\rangle\}$ , see introduction.

Because the orthogonality is not constraint a unitary transformation matrix needs to be constructed from the eigenvectors of the overlap[12]

$$\tilde{O}_{ij} = \langle \psi_i | \psi_j \rangle. \quad (14)$$

For small systems, the associated computational effort is negligible but for larger systems it is notable, particularly, as it significantly hampers scaling at large core counts.

In the original code the LAPACK `dspev` solver was executed on the MPI root rank and the eigenvectors were broadcasted to all MPI tasks.

We improved the scaling and the performance by replacing the packed LAPACK routine `dspev` with the unpacked version using the divide-and-conquer algorithm implemented in the LAPACK routine `dsyed`.

This by itself lead to a significant speed up but the problem still constitutes a non-scaling part of the overall calculation.

Employing the parallel Lanczos method, which is already implemented in CPMD [36], failed to outperform the LAPACK routine, so we abandoned it.

For systems of  $N \gtrsim 2000$  the problem size is large enough that one can consider to use MPI-OpenMP parallel eigenvalue solver, like EigenEXA [37], ScaLAPACK [38], or ELPA.[31] We currently only have implemented an interface to the ELPA eigenvalue solver, which is called on a subset of all available MPI tasks. The achievable speed up, however, is of course strongly dependent on the parallel setup and on the machine used.

Apart from speeding up the eigenvalue problem, the original implementation of the USPP Car-Parrinello MD scheme applied this transformation only after a user defined threshold of the overlap (14) is reached [12].

We reimplemented the missing equations and also benchmarked the performance impact of a threshold of  $10^{-4}$  which is tighter than the recommended threshold of  $10^{-3}$  [12]. In our benchmark calculations the eigenvalue problem has to be solved only every 5th MD step. The corresponding results are presented in Fig. 10 in Section 4.1.

## 4. Results and Discussion

All changes to the code introduced above resulted in an improved performance and scalability. This performance is evaluated by the achievable trajectory length measured in ps per day of walltime, which allows an easy estimate of turnaround times for a given simulation scenario. As a rule of thumb, a performance of 1 ps/day is the minimum needed to achieve results on the order of a few weeks. Below this limit, one will only conduct simulations only under exceptional circumstances. On the other hand, performances largely exceeding 10 ps/day will open the possibility to conduct many computer experiments on a given system, due to the short turn-around times. We also provide the performance in s/MD step. This quantity can be compared to a wave-function update in an SCF cycle. Such a wave-function update is roughly 20% faster than a Car-Parrinello MD step, since it does not involve calculations of ionic forces. A performance of 1 ps/day equals 12.5 s/MD step or roughly 10 s/SCF cycle. For very large systems exceeding 512 water



Table 1: For a given number of nodes the table lists the OpenMP threads and the number of `cp_groups`  $g$  yielding the shortest time per MD step and the corresponding best performance.

nodes	cores	threads	$g$	time s	perf. ps / day
1	48	4	1	3.61	3.47
2	96	4	1	1.84	6.79
3	144	6	1	1.31	9.57
4	192	8	1	1.03	12.1
5	240	6	1	0.840	14.9
6	288	12	1	0.738	17.0
7	336	8	1	0.647	19.4
8	384	6	1	0.569	22.0
10	480	12	1	0.500	25.1
11	528	12	1	0.472	26.6
12	576	12	1	0.439	28.5
16	768	12	1	0.345	36.4
20	960	8	1	0.316	39.6
24	1152	12	1	0.300	41.8
30	1440	12	1	0.250	50.1
32	1536	12	2	0.228	54.9
64	3072	12	2	0.167	75.2
128	6144	12	4	0.140	89.6
240	11520	24	8	0.130	96.5

molecules, this is a better quantity as here most DFT calculations are conducted to optimize geometries or even just to analyze the band structure of a given system.

#### 4.1. Performance and Scalability of the 256 Water Benchmark System

First, we turn to the benchmark system of 256 water molecules, for which we have already discussed the improvements of the subroutines in Sec. 3. Table 4.1 shows the timings and setup (OpenMP threads, `cp_groups`) with the best performance for the revised CPMD code. With the improved threading support and the `cp_groups` parallelization we achieve a performance increases for up to 240 nodes (11.5 k cores). For most setups 12 OpenMP threads per MPI task yield the best performance, which corresponds to 4 MPI tasks per node. Only for small node counts and the limiting 240 nodes a smaller and larger number of threads, respectively, is preferential. The `cp_groups` parallelization is profitable only for more than 30 nodes and is required to use very large core counts.

Figure 8 shows the scaling data of the revised code given in Tab. 4.1 and compares it to the performance of the original code on a linear scale.

For a single node (48 cores) the revised implementation outperforms the old code by a factor of 2.5. Up to six nodes, the old code is faster in a pure MPI set up and profits from hybrid MPI+OpenMP parallelization only for larger node counts. However, the parallel efficiency drops significantly below 50%, which is often considered a threshold to use the HPC facilities at computing centers.

In contrast, the hybrid MPI+OpenMP parallelization of the new implementation is faster for all node counts. On a single

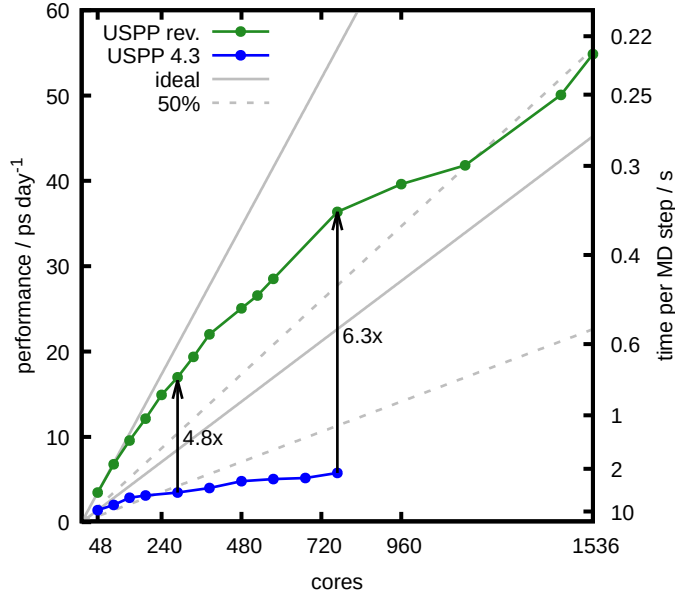


Figure 8: Performance improvement for the 256 water benchmark system with USPP. Blue shows the old and green the new implementation. 50 % efficiency is shown in grey dashed. Please note the linear scale of both axes.

node it uses 4 OpenMP threads per MPI task and 12 OpenMP threads per task at 20 nodes (960 cores). Its performance at 6 nodes is 4.8 times faster and 16 nodes it is more than 6 times faster. The parallel efficiency stays well above a 50 % up to 20 nodes.

At 30 nodes (1440 cores) the efficiency drops slightly below 50 %, however, at 32 nodes (1536 cores) it reclaims the 50 % efficiency barrier by using `cp_groups` parallelism. The achieved performance is about 55 ps/day or less than 0.23 s per MD step. Compared to the old code, this is more than 9 times faster by using just twice the resources.

Despite our focus on the USPP code path, also NCPP calculations profit from our optimizations, particularly due to the batched FFT, see Section 3.5. The log-scaled Figure 9 compares the performance of the original and the revised code for USPP and NCPP, respectively, on the 256 water benchmark system. At low node counts up to 12 the performance improvement of the NCPP code path is 30 % on average. For larger node counts the new batched FFT algorithm plays its strength and retains perfect scaling much longer than the old implementation. Here, the performance improvement is more than 50 % and the parallel efficiency is larger than 50 % even at 108 nodes (5184 cores).

The old USPP implementation was only up to 4 nodes faster than NCPP. Note that for NCPP on a single node the memory was insufficient to store the wave-function FFTs, which are six times larger than for USPP due to the larger PW cutoff. Therefore, we have omitted this point for NCPP and use two nodes for its reference. For the minimal configuration USPP is now 4.5 times more efficient than NCPP in the new implementation, which covers about 80 % of the maximum possible speed up of 5.7 due to the ratio of the number of PW. Thus, the USPP overhead related to the larger number of  $\beta$ -projectors and addi-

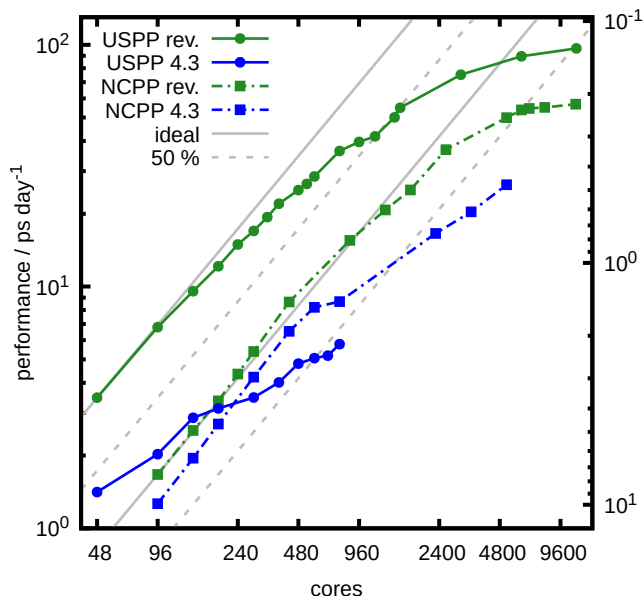


Figure 9: Performance of USPP (solid) and NCPP (dashed) simulations. Blue lines show the old and green the new implementation.

tional terms that have to be computed now seems to be in a well acceptable limit. The scaling of USPP is not as close to ideal as NCPP and drops just below 50 % parallel efficiency after 32 nodes (1536 cores). Nevertheless, it remains faster than than NCPP, outperforming it by 70 % above 5000 cores.

#### 4.2. System Size Dependence

Finally, we consider the scalability and performance depending on a broad range of system sizes. The smallest system of 32 molecules was used as a minimal system to study liquid water and aqueous solutions in the early days of AIMD [39, 40]. The largest system of 2048 water molecules covers 8196 electronic states. For similarly sized systems structure optimizations at DFT level are of interest today.

All scaling curves are collected in Figure 10. For the smallest system of 32 molecules we reach a performance of more than 1 ns/day with 20 nodes, a performance scale previously only known from force-field based MD simulations. Of course, the parallel efficiency at large core counts is rather poor due to the small size of the system.

For 64 molecules one readily reaches more than 264 ps/day with 5 nodes (240 cores) at a good parallel efficiency. The next system, consisting of 128 molecules we reach a performance of 121 ps/day with just 12 nodes before dropping below 50 % parallel efficiency. In the scaling limit we can reach a performance exceeding 590 ps/day and 284 ps/day respectively. A system twice the size of our benchmark system at 512 molecules requires 1440 cores to reach more than 10 ps/day with while the maximum achievable performance is greater than 20 ps/day.

Very large systems test the limits of the implementation. At 1024 molecules we find a good scaling up to 2304 cores reaching about 2,5 ps/day and more than 7 ps/day in the scaling limit. This shows that our code revisions elevate this system size to a

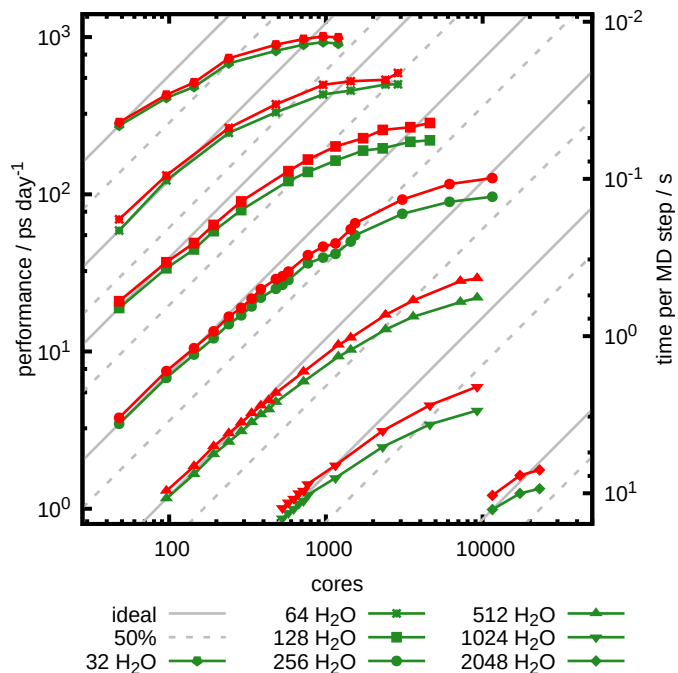


Figure 10: Performance and scaling of the revised CPMD USPP code for water systems of increasing size (green curves). Minimal core set ups for each system have been chosen due to memory restrictions. Red lines show the impact of additionally reimplementing the threshold to trigger the eigenvalue problem.

performance sufficient for production runs. Starting with simulations of this size, we also see additional subroutines hampering scaling that do not play a role for smaller systems and which leave room for further improvements. One example is the calculation of the inverse root  $T = O^{-1/2}$  of (9).  $T$  is calculated as the inverse of a Cholesky factor by subsequent calls to the Lapack routines `dpotrf` and `dtrtri` on the MPI root rank. A possible enhancement would be the adaption of the blocked Gram-Schmidt orthogonalization method implemented by Bekas for NCPP to the USPP formalism. [41]

For the largest benchmark system of 2048 molecules we found only three stable simulation setups, because the memory requirements were exceeding the available node memory of 96 GB. Yet we were able to reach a performance of more than 1.7 ps/day, making it accessible for production runs.

Particularly these large systems are hampered by solving the eigenvalue problem described in Sec. 3.6. The red curves show the advantage of restoring the original Hutter implementation where the respective function is called on average only every 5th MD step due to the active threshold. Since the eigenvalue problem too small to be as efficiently parallelized as the rest of the code its impact is most pronounced in the scaling limit, as Amdahl's law predicts.[42] For the larger systems, the speedup is on the order of up to 30 %.

Note that DFT does not scale linearly with the system size  $N$  but rather with  $N^\alpha$ ,  $\alpha > 1$ . From respective minimal configurations presented in Fig. 10 we calculated an effective single node performance for each system size. We find that the USPP code path scales with  $\sim N^{2.6}$ .

Compared to our intermediate results acquired on

SuperMUC-Phase2[18] we were able to adopt our routines to the new SuperMUC-NG and obtain now at least twice the performance for small systems and close to ten times higher performance with the largest benchmark system of 2048 water molecules. The scalability improvement was mainly achieved by the now communication free `rn1sm2` routine described in Section 3.2 whereas the improved core performance was just obtained by using highly optimized BLAS routines all over the code at did not require any further tuning on our side.

## 5. Summary and Outlook

Optimizing AIMD for HPC systems is a challenging task despite its high computational intensity. One obstacle is the large amount of data needed to describe the electronic states, which needs to be distributed among the nodes. Still, the electronic states are tightly coupled requiring *all-to-all* data exchange between the nodes, which is a large disadvantage compared to scalable nearest neighbour communication used by many grid based codes. Also instead of a single monolithic kernel, AIMD has many inter-dependent compute tasks. Due to the data distribution each task requires a different parallelization strategy which makes the whole optimization process particularly tedious.

We have greatly enhanced the performance and scalability of the USPP AIMD implementation in CPMD. All rate limiting routines have been revised and improved and communication patterns have been reworked. For a number of routines we have shown that overlapping computation and communication is indeed profitable when reaching the scaling limit. In the revised code the distributed matrix-matrix multiplications in the `rn1sm` routine and the 3-*d* FFTs still require the largest computational effort and determine the limits of scalability. The algorithmic changes we have introduced have pushed these limits farther out and allow more cores to work on a given problem.

With the code improvements we have not only increased the reasonably accessible system sizes for CPMD simulations by at least one order of magnitude along with much shorter turn-around times but also largely stretched the accessible time range, bringing multi nanosecond CPMD simulations down to just a few days of simulation for systems up to 256 water molecules.

Further development will be on the methods side, implementing Hartree Fock exchange [43] together with wave-function localization methods[44, 45]. Due to our high usage of performance libraries, we are also confident that porting our routines to heterogenous HPC cluster with accelerators will be straight forward.

## Acknowledgments

This work has been funded by state of Bavaria (KONWIHR software initiative). The authors gratefully acknowledge the compute resources and support provided by the Erlangen Regional Computing Center (RRZE). Technical support for optimization has been granted by the PRACE High Level Support

team (HLST) at the Leibniz Supercomputing Centre (LRZ). Computer time for benchmarking was generously provided by the LRZ during the reliability-testing phase of SuperMUC-NG (project pn69qo).

## References

- [1] J. Hutter, A. Curioni, Car-parrinello molecular dynamics on massively parallel computers., *Comput. Phys. Commun.* 6 (2005) 1788–1793.
- [2] D. Marx, J. Hutter, *Ab Initio Molecular Dynamics: Basic Theory and Advanced Methods*, Cambridge University Press, Cambridge, 2009.
- [3] J. Hutter, A. Alavi, T. Deutsch, M. Bernasconi, S. Goedecker, D. Marx, M. Tuckerman, M. Parrinello, CPMD: Car-Parinello Molecular Dynamics, version 4.1, © IBM Corp 1990-2019, © MPI für Festkörperforschung Stuttgart 1997-2001 (2019). URL <http://www.cpmc.org>
- [4] Message Passing Interface Forum, MPI: A Message-Passing Interface Standard, Version 3.1, University of Tennessee, Knoxville, Tennessee 37831 (June 2015).
- [5] OpenMP Architecture Review Board, OpenMP Application Programming Interface, 4th Edition (2002).
- [6] V. Weber, A. C. I. Malossi, I. Tavernelli, T. Laino, C. Bekas, M. Modani, N. Wilner, T. Heller, A. Curioni, First experiences with ab initio molecular dynamics on openpower: The case of cpmd, in: M. Taufer, B. Mohr, J. M. Kunkel (Eds.), *High Performance Computing*, Springer International Publishing, Cham, 2016, pp. 228–234.
- [7] W. Andreoni, A. Curioni, New advances in chemistry and materials science with cpmd and parallel computing, *Parallel Computing* 26 (7) (2000) 819 – 842. doi:10.1016/S0167-8191(00)00014-4.
- [8] J. Hutter, A. Curioni, Dual-level parallelism for ab initio molecular dynamics: Reaching teraflop performance with the cpmd code, *Parallel Computing* 31 (1) (2005) 1 – 17. doi:10.1016/j.parco.2004.12.004.
- [9] H. Hellmann, A new approximation method in the problem of many electrons, *J. Chem. Phys.* 3 (1) (1935) 61–61. doi:10.1063/1.1749559.
- [10] D. Vanderbilt, Soft self-consistent pseudopotentials in a generalized eigenvalue formalism, *Phys. Rev. B* 41 (1990) 7892–7895.
- [11] K. Laasonen, A. Pasquarello, R. Car, C. Lee, D. Vanderbilt, Car-parrinello molecular dynamics with vanderbilt ultrasoft pseudopotentials, *Phys. Rev. B* 47 (16) (1993) 10142–10153.
- [12] J. Hutter, M. Tuckerman, M. Parrinello, Integrating the car-parrinello equations. iii. techniques for ultrasoft pseudopotentials, *The Journal of Chemical Physics* 102 (2) (1995) 859–871. doi:10.1063/1.469201.
- [13] L. S. Blackford, J. Demmel, J. Dongarra, I. Duff, S. Hammarling, G. Henry, M. Heroux, L. Kaufman, A. Lumsdaine, A. Petitet, R. Pozo, K. Remington, R. C. Whaley, An updated set of Basic Linear Algebra Subprograms (BLAS), *ACM Transactions on Mathematical Software* 28 (2) (2002) 135–151.
- [14] E. Anderson, C. B. Z. Bai, J. Demmel, J. Dongarra, J. du Croz, A. Greenbaum, S. Hammarling, A. Mckenney, D. Sorensen, *Lapack: A portable linear algebra library for high-performance computers*, Tech. rep., Computer Science Dept., University of Tennessee, Knoxville (1990).
- [15] W. H. Press, B. P. Flannery, S. A. Teukolsky, W. T. Vetterling, *Numerical Recipes in C*, Cambridge University Press, Cambridge, 1988.
- [16] OpenMP Architecture Review Board, OpenMP Application Programming Interface, 5th Edition (2018).
- [17] V. Weber, C. Bekas, T. Laino, A. Curioni, A. Bertsch, S. Futral, Shedding light on lithium/air batteries using millions of threads on the bg/q supercomputer, in: *2014 IEEE 28th International Parallel and Distributed Processing Symposium*, 2014, pp. 735–744. doi:10.1109/IPDPS.2014.81.
- [18] T. Klöffel, B. Meyer, G. Mathias, Boosting the scalability of car-parrinello molecular dynamics simulations for multi- and manycore architectures, Supercomputing, Dallas, Texas USA. URL [https://sc18.supercomputing.org/proceedings/tech\\_poster/tech\\_poster\\_pages/post189.html](https://sc18.supercomputing.org/proceedings/tech_poster/tech_poster_pages/post189.html)
- [19] J. Treibig, G. Hager, G. Wellein, Likwid: A lightweight performance-oriented tool suite for x86 multicore environments, in: *Proceedings of the 2010 39th International Conference on Parallel Processing Workshops*,

- ICPPW '10, IEEE Computer Society, Washington, DC, USA, 2010, pp. 207–216. doi:10.1109/ICPPW.2010.38.
- [20] C. Guillen, W. Hesse, M. Brehm, The persyst monitoring tool, in: L. Lopes, J. Žilinskas, A. Costan, R. G. Cascella, G. Kecskemeti, E. Jeannot, M. Cannataro, L. Ricci, S. Benkner, S. Petit, V. Scarano, J. Gracia, S. Hunold, S. L. Scott, S. Lankes, C. Lengauer, J. Carretero, J. Breitbart, M. Alexander (Eds.), Euro-Par 2014: Parallel Processing Workshops, Springer International Publishing, Cham, 2014, pp. 363–374.
- [21] Intel Corporation, Intel Fortran Compiler 19.0 Developer Guide and Reference (2019).
- [22] M. Heyden, J. Sun, S. Funkner, G. Mathias, H. Forbert, M. Havenith, D. Marx, Dissecting the thz spectrum of liquid water from first principles via correlations in time and space, Proc. Natl. Acad. Sci. USA 107 (2010) 12068–12073.
- [23] A. Hassanali, J. Cuny, V. Verdolino, M. Parrinello, Aqueous solutions: state of the art in ab initio molecular dynamics., Philosophical transactions. Series A, Mathematical, physical, and engineering sciences 372 2011 (2014) 20120482.
- [24] A. P. Gaiduk, T. A. Pham, M. Govoni, F. Paesani, G. Galli, Electron affinity of liquid water, Nat. Commun. 9 (1) (2018) 247. doi:10.1038/s41467-017-02673-z.
- [25] V. Rozsa, D. Pan, F. Giberti, G. Galli, Ab initio spectroscopy and ionic conductivity of water under earth mantle conditions, Proc. Natl. Acad. Sci. USA 115 (27) (2018) 6952–6957. doi:10.1073/pnas.1800123115.
- [26] L. Zheng, M. Chen, Z. Sun, H.-Y. Ko, B. Santra, P. Dhuvad, X. Wu, Structural, electronic, and dynamical properties of liquid water by ab initio molecular dynamics based on scan functional within the canonical ensemble, J. Chem. Phys. 148 (16) (2018) 164505. doi:10.1063/1.5023611.
- [27] J. P. Perdew, K. Burke, Y. Wang, Generalized gradient approximation for the exchange-correlation hole of a many-electron system, Phys. Rev. B 54 (1996) 16533–16539. doi:10.1103/PhysRevB.54.16533.
- [28] S. Grimme, Semiempirical GGA-type density functional constructed with a long-range dispersion correction, J. Comput. Chem. 27 (15) (2006) 1787–1799. doi:10.1002/jcc.20495.
- [29] Intel Corporation, Intel Math Kernel Library: Developer Reference 2019, 095th Edition (2019).
- [30] Intel Corporation, Intel MPILibrary (Developer Reference) (2019).
- [31] A. Marek, V. Blum, R. Johanni, V. Havu, B. Lang, T. Auckenthaler, A. Heinecke, H.-J. Bungartz, H. Lederer, The elpa library: scalable parallel eigenvalue solutions for electronic structure theory and computational science, J. Phys.: Condens. Matter 26 (21) (2014) 213201.
- [32] N. Troullier, J. L. Martins, Efficient pseudopotentials for plane-wave calculations, Phys. Rev. B 43 (3) (1991) 1993–2005.
- [33] CP2K.org, CP2K Benchmark Suite - CP2K Open Source Molecular Dynamics. URL <https://www.cp2k.org/performance>
- [34] S. Goedecker, M. Boulet, T. Deutsch, An efficient 3-dim FFT for plane wave electronic structure calculations on massively parallel machines composed of multiprocessor nodes, Computer Physics Communications 154 (2) (2003) 105–110. doi:10.1016/S0010-4655(03)00287-X.
- [35] M. Frigo, S. G. Johnson, The design and implementation of FFTW3, Proc. IEEE 93 (2) (2005) 216–231, special issue on “Program Generation, Optimization, and Platform Adaptation”.
- [36] C. Bekas, A. Curioni, W. Andreoni, Atomic wavefunction initialization in ab initio molecular dynamics using distributed lanczos, Parallel Computing 34 (6) (2008) 441 – 450.
- [37] T. Imamura, S. Yamada, M. Machida, Development of a high performance eigensolver on the petascale next generation supercomputer system, Progress in Nuclear Science and Technology 2 (2011) 643–650.
- [38] D. Gimnez, C. Jimnez, M. J. Majado, N. Marn, A. Martn, Solving eigenvalue problems on networks of processors, in: V. Herndez, J. M. L. M. Palma, J. J. Dongarra (Eds.), Vector and Parallel Processing VEC- PAR'98, Springer Berlin Heidelberg, Berlin, Heidelberg, 1999, p. 8599.
- [39] M. Tuckerman, K. Laasonen, M. Sprik, M. Parrinello, Ab initio molecular dynamics simulation of the solvation and transport of hydronium and hydroxyl ions in water, J. Chem. Phys. 103 (1995) 150–161.
- [40] D. Marx, M. E. Tuckerman, J. Hutter, M. Parrinello, The nature of the hydrated excess proton in water, Nature 397 (1999) 601–604.
- [41] C. Bekas, A. Curioni, Very large scale wavefunction orthogonalization in density functional theory electronic structure calculations, Computer Physics Communications 181 (6) (2010) 1057 – 1068. doi:10.1016/j.cpc.2010.02.013.
- [42] G. M. Amdahl, Validity of the single processor approach to achieving large scale computing capabilities, reprinted from the afips conference proceedings, vol. 30 (atlantic city, n.j., apr. 1820), afips press, reston, va., 1967, pp. 483485, when dr. amdahl was at international business machines corporation, sunnyvale, california, IEEE Solid-State Circuits Society Newsletter 12 (3) (2007) 19–20. doi:10.1109/N-SSC.2007.4785615.
- [43] J. P. Perdew, M. Ernzerhof, K. Burke, Rationale for mixing exact exchange with density functional approximations, J. Chem. Phys. 105 (22) (1996) 9982–9985. doi:10.1063/1.472933.
- [44] A. Damle, L. Lin, L. Ying, Compressed representation of kohnsham orbitals via selected columns of the density matrix, J. Chem. Theory Comput. 11 (4) (2015) 14631469, pMID: 26574357. doi:10.1021/ct500985f.
- [45] N. Marzari, D. Vanderbilt, Maximally localized generalized wannier functions for composite energy bands, Phys. Rev. B 56 (1997) 12847–12865. doi:10.1103/PhysRevB.56.12847.